XL CILAMCE
IBERO-LATIN AMERICAN CONGRESS ON COMPUTATIONAL METHODS IN ENGINEERING
NOVEMBER 11-14, 2019
Praiamar Natal Hotel & Convention
Natal, RN-BRAZIL

ISOGEOMETRIC BOUNDARY ELEMENT ANALYSIS APPLIED TO ELASTIC PROBLEMS

Fernando Morais de Loyola
Éder Lima de Albuquerque
f.loyola91@gmail.com
eder@unb.br
Universidade de Brasília
Faculdade de Tecnologia, 70910-900, Brasília-DF, Brazil
Lucas Silveira Campos
lucas.s.campos@ufes.br
Universidade Federal do Espírito Santo
Centro Tecnológico, 29075-910, Vitória-ES, Brazil

Abstract. The main idea of this work is to solve elastic problems using Isogeometric Boundary Element Formulation. A standard BEM with quadratic elements is also used in order to compare the efficiency of both methods. In isogeometric method, instead of using polynomial shape functions, both geometry and analysis use non-uniform rational B-splines (NURBS). NURBS are widely used for geometric modelling in CAD software and, due to this, makes the discretization of the geometry unnecessary. One obvious advantage of using this type of B-splines is that it can perfectly describe complex shapes, making results more accurate. The most important feature, however, is the decrease in the amount of user's work, because the most time-consuming step – mesh generation – is reduced or even eliminated. In order to easy implementation in existing boundary element codes, NURBS are transformed into Bézier curves (Bézier decomposition). So, each Bézier curve can be viewed as a boundary element in a conventional boundary element implementation.

It is worth mentioning that displacement and tractions have their values solved at the control points and NURBS curves do not necessarily touch them. For the definition of collocation points, Gauss-Legendre collocation points are used in this study. Therefore, a transformation matrix, which uses basis functions for relating values at control and at collocation points, is needed. The equation for isogeometric BEM is defined in terms of the control points and, after applying the transformation, can be solved as the standard BEM. Lastly, numerical and analytical solutions are compared in order to validate the method.

Keywords: Boundary Element Method, Isogeometric Formulation, Bézier Decomposition, Elasticity

1 Introduction

Since the concept of isogeometric analysis (IGA) was introduced by Hughes et al. [1], it has received attention from many researchers, given that it can improve the established analysis process. Among other contributions is a decrease in the amount of user's work, because the most time-consuming step – mesh generation – is reduced or even eliminated. To evidence isogeometric analysis advantage over isoparametric, they are compared in this study.

Four years after the previous work, a book has been published Cottrell et al. [2] about IGA. The novelty about this approach is that instead of using polynomial functions to discretise geometry and unknown fields, IGA uses the same basis as CAD (Computer Aided Design) softwares, which are often NURBS (Non-Uniform Rational B-splines), but can also be T-splines or others. One of the reasons that NURBS are widely used by CAD is because they can exactly describe complex geometries that are only approximated using polynomials. Although it has been initially presented with Finite Element Method (FEM) as in Cottrell et al. [2], isogeometric Boundary Element Method (IGABEM) for elastostatic was developed in Simpson et al. [3, 4], in which NURBS are used to approximate the geometry along with the displacement and traction fields around the boundary. Works such as Cabral et al. [5, 6] already used B-splines as basis functions in BEM, however with no concern about integration with CAD.

Other applications of isogeometric such as contact mechanics are presented by Temizer et al. [7, 8], Lu [9], shells Kiendl et al. [10, 11], Benson et al. [12], Deng et al. [13]. More recent studies such as Sun et al. [14, 15, 16] use IGABEM in acoustics, potential and structural optimization.

Sun et al. [17] uses IGABEM with Bézier decomposition for solving crack propagation problems. In the present study, IGABEM is also used with Bézier decomposition to facilitate incorporating NURBS into existing boundary element codes for solving elastic problems.

2 Elasticity

Firstly, we must define what problem to solve. For elastostatics, under the conditions of equilibrium, the summation of all forces on the elastic body equals zero, i.e.:

$$\sigma_{ij,j} + b_i = 0, \tag{1}$$

where $i, j = 1, 2, 3$, subscript $_{,j}$ denotes differentiation with respect to x_j, σ_{ij} is the Cauchy stress tensor and b_i are body forces. These external and internal loads induce linear and angular displacements in the body. Assuming small displacements, strains ϵ_{ij} are

$$\epsilon_{ij} = \frac{1}{2}(u_{i,j} + u_{j,i}) \tag{2}$$

where u_i represents displacement. Assuming an elastic, homogeneous and isotropic material and using the constitutive equation (Hooke's Law),

$$\sigma_{ij} = \lambda \epsilon_{kk} \delta_{ij} + 2\nu \epsilon_{ij}, \tag{3}$$

where λ is the Lamé constant $\lambda = \frac{2\nu\mu}{1-2\nu}$, $\mu = \frac{E}{2(1+\nu)}$ is the shear modulus, E is the Young modulus, ν is Poisson's ratio and δ_{ij} is the Kronecker delta, defined as

$$\delta_{ij} = \begin{cases} 1 & \text{if } i = j \\ 0 & \text{if } i \neq j. \end{cases} \tag{4}$$

Now, consider a body with domain Ω and boundary Γ as represented in Fig. 1. It can have two different types of boundary conditions, i.e., in Γ_u displacements are known and in Γ_t, tractions are known:

$$\begin{aligned} u_i &= \bar{u}_i \; on \; \Gamma_u, \\ t_i &= \bar{t}_i \; on \; \Gamma_t, \end{aligned} \tag{5}$$

where

$$\Gamma = \Gamma_u \cup \Gamma_t \; and \; \Gamma_u \cap \Gamma_t = \emptyset. \tag{6}$$

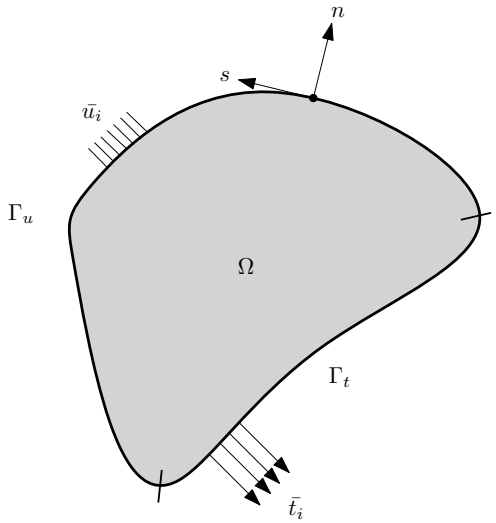

Figure 1. Definition of domain.

Our problem can be staded as follows: given $\bar{u}_i$, $\bar{t}_i$ and b_i, find u_i that satisfies Eq. (1).

3 Standard BEM

Before introducing the concept of isogeometric BEM, it is important to show the isoparametric formulation, also used in this study for comparison. In this case, elements can be constant, linear, quadratic etc. This section is aimed at outlining standard BEM, not presenting a detailed derivation of the entire method. For the latter purpose, references such as Brebbia and Dominguez [18], Katsikadelis [19], Cruse [20] can be useful.

Let Ω be the domain of a body with boundary Γ. It is possible to define two points P and Q, namely source point and field point, respectively. They are separated by a distance r

$$r := ||P - Q|| \tag{7}$$

as in Fig. 2.

Starting with the constraint equation, which relates the values of the surface displacements u_i to the surface tractions t_i,

$$C_{ij}(P)u_j(P) + \int_\Gamma T_{ij}(P,Q)u_j(Q)d\Gamma = \int_\Gamma U_{ij}(P,Q)t_j(Q)d\Gamma \tag{8}$$

where u_j and t_j are the components of displacement and traction, U_{ij} and T_{ij} are displacement and traction fundamental solutions, respectively and C_{ij} depends on geometry as

$$C_{ij} = \begin{cases} 1 & \text{if } P \in \Omega \\ \frac{\theta_{int}}{2\pi} & \text{if } P \in \Gamma \\ 0 & \text{if } P \notin (\Omega \vee \Gamma). \end{cases} \tag{9}$$

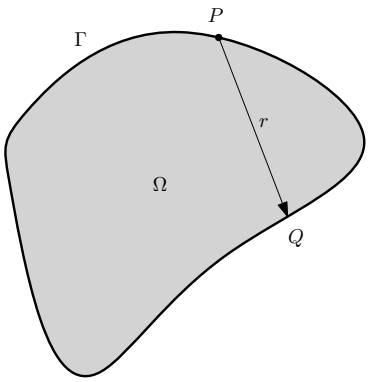

Figure 2. Domain, boundary with source and field points.

When the source point lies on a smooth part of boundary, C_{ij} is

$$C_{ij} = \frac{\theta_{int}}{2\pi} = \frac{\pi}{2\pi} = \frac{1}{2}. \tag{10}$$

The first integral of Eq. (8) must be evaluated in Cauchy Principal Value (CPV) due to the strong singularity $\mathcal{O}(r^{-1})$ in T_{ij} kernel. As Eq. (8) is in continuous form, it does not suit computational implementation yet. Thus, the next step is to discretise by dividing the real boundary into elements with local coordinate $\xi \in [-1, 1]$. After doing the discretisation, geometry and unknown fields can be approximated as

$$x_e(\xi) = \sum_{k=1}^{m} N_k(\xi) x_k, \tag{11}$$

$$u_e(\xi) = \sum_{k=1}^{m} N_k(\xi) u_k, \tag{12}$$

$$t_e(\xi) = \sum_{k=1}^{m} N_k(\xi) t_k, \tag{13}$$

where x_k, u_k, and t_k are nodal coordinates, displacements and tractions, respectively; m is the number of nodes per element (such as 2 for linear or 3 for quadratic elements); $N_k(\xi)$ are the Lagrangian polynomial basis functions; subscript $_e$ denotes that the value is for element e.

In order to allow computational implementation, it is necessary to map global coordinates into local coordinates, with value $[-1, 1]$ as stated previously, aiming to apply the Gaussian quadrature. The jacobian of this transformation is given by

$$J(\xi) = \sqrt{\left(\frac{\partial x_1}{\partial \xi}\right)^2 + \left(\frac{\partial x_2}{\partial \xi}\right)^2}. \tag{14}$$

Substituting Eqs. (11) to (13) in Eq. (8), it is possible to write the discretised displacement boundary integral equation as

$$\sum_{k=1}^{m} C_{ij}(P)u_j(P) + \sum_{e=1}^{ne}\sum_{k=1}^{m}\left[\underbrace{\int_{-1}^{1} T_{ij}(P,Q)N_k(\xi)J(\xi)d\xi}_{H'_{ij}}\right] u_j^{ek} = \sum_{e=1}^{ne}\sum_{k=1}^{m}\left[\underbrace{\int_{-1}^{1} U_{ij}(P,Q)N_k(\xi)J(\xi)d\xi}_{G_{ij}}\right] t_j^{ek}. \tag{15}$$

where $H_{ij} = H'_{ij} + C_{ij}$.

After considering the collocation point P over each boundary nodal point, it is possible to obtain a system with N equations, where N is the number of degrees of freedom. This set of equations can be written in matrix form as

$$\mathbf{Hu} = \mathbf{Gt}, \tag{16}$$

where $\mathbf{H}$ and $\mathbf{G}$ have values of fundamental solutions T_{ij} and U_{ij}, $\mathbf{t}$ and $\mathbf{u}$ contain traction and displacements, respectively. When dealing with a problem, often some traction and some displacement are unknowns, and by using some algebra, it is possible to isolate these unknowns in a vector $\mathbf{x}$. Hence, Eq. (16) becomes:

$$\mathbf{Ax} = \mathbf{b} \tag{17}$$

and only one solution is possible.

4 B-splines and NURBS

IGA allows using the same basis functions for modelling the geometry and analyzing the problem. Thus, it is important to present the basic concepts of B-splines and NURBS. For a more detailed description, one can see Piegl and Tiller [21]. Throughout this section, it is going to be clear that NURBS are a generalization of B-splines, so we start by presenting the latter definition.

B-splines

Given a knot vector $\boldsymbol{U} = (u_0, u_1, \cdots, u_{n+p+1})$ where $u_i \in R$ is the i-th knot, i is the knot index, $i = 1, 2, \cdots, n+p+1$, p is the order of the polynomial and n is the number of functions used to generate the B-spline. By definition, the basis of order zero (p = 0) is

$$N_{i,0}(t) = \begin{cases} 1 & \text{if } u_i \leq t < u_{i+1} \\ 0 & \text{otherwise} \end{cases} \tag{18}$$

Functions are recursively calculated as in Eq. (19), known as *Cox-de-Boor recursive formula*:

$$N_{i,k}(t) = \frac{(t-u_i)}{u_{i+k-1}-u_i} N_{i,k-1}(t) + \frac{(u_{i+k}-t)}{u_{i+k}-u_{i+1}} N_{i+1,k-1}(t). \tag{19}$$

Number of knots m, number of control points (CP), k, and order n are related as $m = k + n + 1$. A B-spline curve can be described as

$$P(t) = \sum_{i=1}^{n+1} B_i N_{i,k}(t)\,, \quad t_{min} \leq t \leq t_{max}\,, \quad 2 \leq k \leq n+1. \tag{20}$$

NURBS

After describing B-splines, NURBS are easily defined. Before presenting the formal definition, however, it is interesting to explain why we chose to use NURBS instead of B-splines in this study. When describing a quarter-circle using B-splines three control points, for example, a large discrepancy is seen between the interpolated curve and the exact, according to Simpson et al. [3]. If NURBS are used, the circle is exactly described with the same number of control points, in addition to a weight associated with each CP.

A NURBS is a Non-Uniform Rational B-spline and it is defined as

$$P(t) = \frac{\sum_{i=1}^{n+1} B_i N_{i,k}(t) w_i}{\sum_{i=1}^{n+1} N_{i,k}(t) w_i} = \sum_{i=1}^{n+1} B_i R_{i,k}(t), \tag{21}$$

where

$$R_{i,k}(t) = \frac{N_{i,k}(t) w_i}{\sum_{i=1}^{n+1} N_{i,k}(t) w_i} \tag{22}$$

is the rational basis function, $N_{i,p}(t)$ is the B-splines basis function and w_i is the weight associated with the i-th control point. Note that if all weights are equal to one ($w_i = 1 \; \forall \; i$), the NURBS curve becomes a B-spline.

5 Bézier decomposition

As presented by Borden et al. [22] and used in Sun et al. [17] for crack propagation, one can obtain a Bézier decomposition inserting repeated knots in all knots of the vector until they have multiplicity equal to the curve degree ($p + 1$). For each inserted knot, the continuity of basis function is reduced while the curve itself remains unchanged. The resulting basis is decomposed in a set of Bézier elements in which every element corresponds to a knot span in the original knot vector. The Bézier decomposition operator provides a mapping from a piecewise Bernstein polynomial basis onto a NURBS basis. For a better understanding of the Bézier extraction consider Figs. 3 and 4.

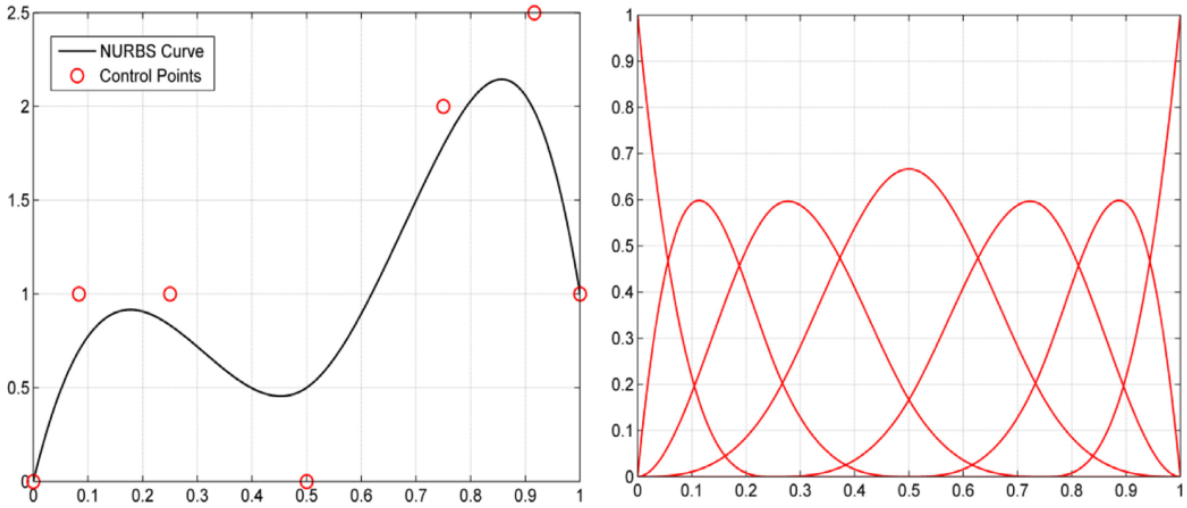

Figure 3. The 3 order polynomial curve and 7 control points and respective B-splines basis functions Sun et al. [17].

Considering two knot vectors, the first one $\boldsymbol{U}_1 = (0\ 0\ 0\ 0\ \frac{1}{4}\ \frac{1}{2}\ \frac{3}{4}\ 1\ 1\ 1\ 1)$ for Fig. 3 and the second one $\boldsymbol{U}_2 = (0\ 0\ 0\ 0\ \frac{1}{4}\ \frac{1}{4}\ \frac{1}{4}\ \frac{1}{2}\ \frac{1}{2}\ \frac{1}{2}\ \frac{3}{4}\ \frac{3}{4}\ \frac{3}{4}\ 1\ 1\ 1\ 1)$ for Fig. 4 after the Bézier decomposition process. It is important to note that the curve remains the same, despite the higher number of control points. As this is

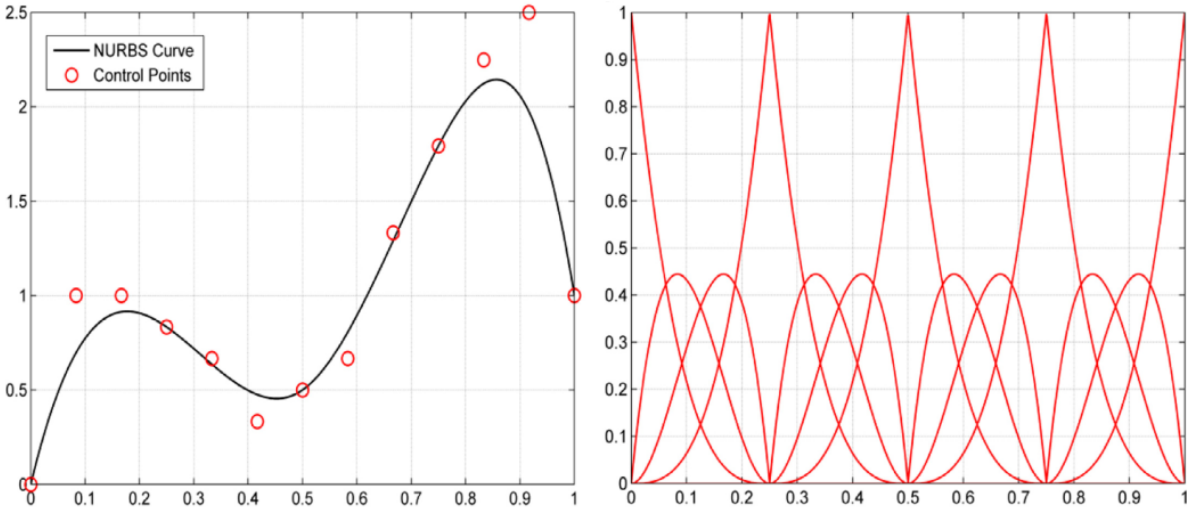

Figure 4. The 3 order polynomial curve and 13 control points and respective Bernstein basis functions Sun et al. [17].

a 3^{rd} order polynomial, a Bézier curve is defined for each 4 control points, resulting in 4 curves in total, taking into consideration that two adjacent curves share a control point. In other words, the last control point of n-th curve is the first control point of the $(n+1)$-th curve.

6 Results

This chapter presents examples used for validating the code, comparing IGABEM with standard BEM using quadratic elements and both with analytical results for elastic problems.

Displacement norms were used for estimating error. Root Mean Square Error ($RMSE$), which has been used for this comparison, can be defined as:

$$RMSE = \sqrt{\frac{1}{N}\sum_{j=1}^{N}[u_{numerical} - u_{analytical}]^2} \tag{23}$$

where N is the number of nodes.

6.1 A thick-walled tube

A thick-walled tube is the first example, with only a quarter of it being modelled as in Fig. 5. The tube is assumed to be in plane strain state. Geometric and material properties can be seen in Table 1.

Table 1. Geometric and material properties - tube.

Property	Symbol	Value
Inner Radius	R_a	50 mm
Outer Radius	R_b	100 mm
Young's Modulus	E	200 GPa
Poisson's Coefficient	ν	$0,32$
Pressure	P	100 N/mm

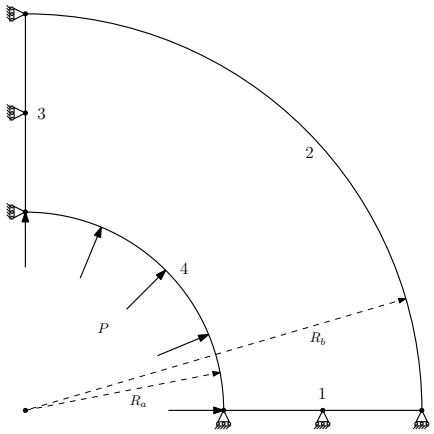

Figure 5. Boundary conditions of problem 1.

Given this problem's symmetry, only a quarter of the tube needs to be modelled. According to Timoshenko et al. [23], the analytical solution for radial displacement u_r is:

$$u_r = \frac{(1+\nu)pa^2}{E(b^2-a^2)}\left[(1-2\nu)r + \frac{b^2}{r}\right] \tag{24}$$

Standard BEM

For the standard isoparametric simulation, 5 different meshes were used (Table 2). They all used quadratic elements, with 3 nodes per element. Numerical results for stresses were also solved, and the color map is in Fig. 6. Deformed configuration was also plotted as the black line.

Table 2. Number of elements per segment for the 5 meshes - tube.

	Elem. per segment					
Mesh	1	2	3	4	**Total nodes**	**DOF**
ST-1	1	3	1	2	14	28
ST-2	2	6	2	4	28	56
ST-3	3	9	3	6	42	84
ST-4	4	12	4	8	56	112
ST-5	5	15	5	10	70	140

Isogeometric BEM

Isogeometric simulation, by its turn, used 10 different meshes (Table 3). Meshes 1 to 5 used p-degree = 2, while meshes 6 to 10 used p-degree = 3. Both of them used h-refinement equals 0, 1, 2, 4 and 8.

Afterwards, displacements were measured over segment 1, for different radius. For this part of the study, only the finest mesh of each method was used, i.e., ST-5 and IT-10. It is noticed that for displacements over the first segment, both methods are accurate compared to analytical solution, as seen in Fig. 7.

The last comparison for this example is regarding error. Meshes ST-5, IT-5 and IT-10 were compared using Eq. (23) for displacement and are shown in Fig. 8. It is easily seen that even with less degrees of freedom, both isogeometric meshes (I-5 and I-10) were consistently more accurate than isoparametric

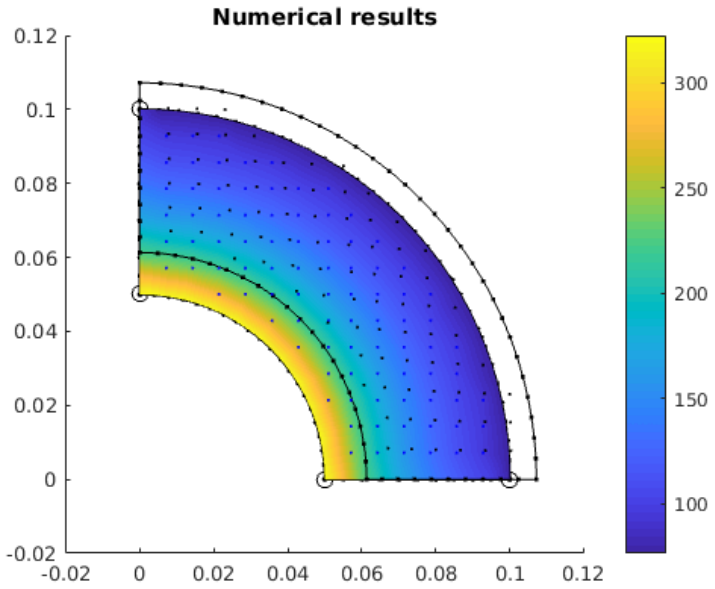

Figure 6. Stresses in tube - numerical results.

Table 3. Number of elements per segment for the 5 meshes.

	Order of segment						
Mesh	1	2	3	4	**p-**	**h-**	**DOF**
IT-1	2	3	2	3	1	0	28
IT-2	2	3	2	3	1	1	36
IT-3	2	3	2	3	1	2	44
IT-4	2	3	2	3	1	4	60
IT-5	2	3	2	3	1	8	92
IT-6	3	4	3	4	2	0	36
IT-7	3	4	3	4	2	1	44
IT-8	3	4	3	4	2	2	52
IT-9	3	4	3	4	2	4	68
IT-10	3	4	3	4	2	8	100

with quadratic elements (S-5). Furthermore, it can be inferred that the two isogeometric meshes have similar behaviour.

6.2 Infinite plate with a circular hole

The second example of this part is an infinite plate with a circular hole, with a P distributed tension along x direction, as in Fig. 9. Geometric and material properties are in Table 4.

One important difference between tube in example 1 and plate in example 2 is related to the stress state. While the former is considered under plane strain state, the latter is simulated as under plane stress state. According to Brebbia and Dominguez [24], "boundary elements for these cases are based on the plane strain approach but can be extended to plane stress if the elastic coefficients are replaced

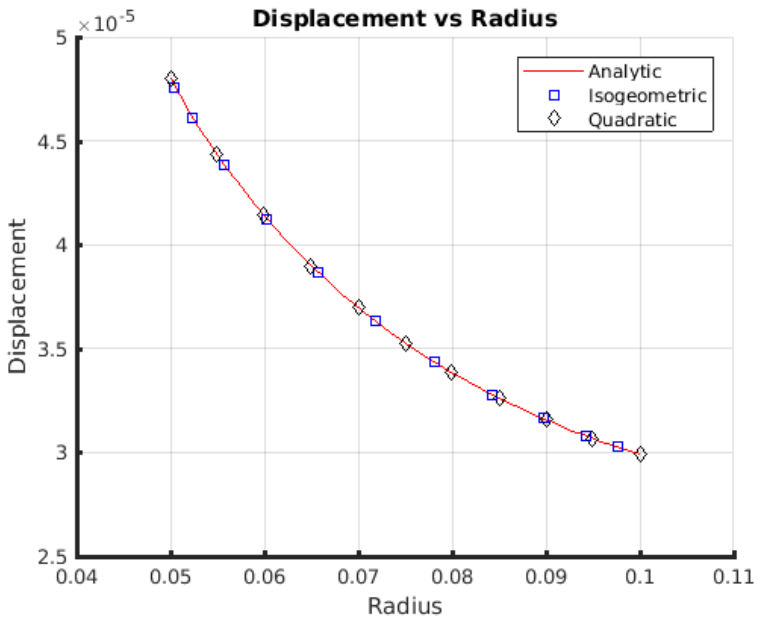

Figure 7. Displacements of the thick-walled tube discretization.

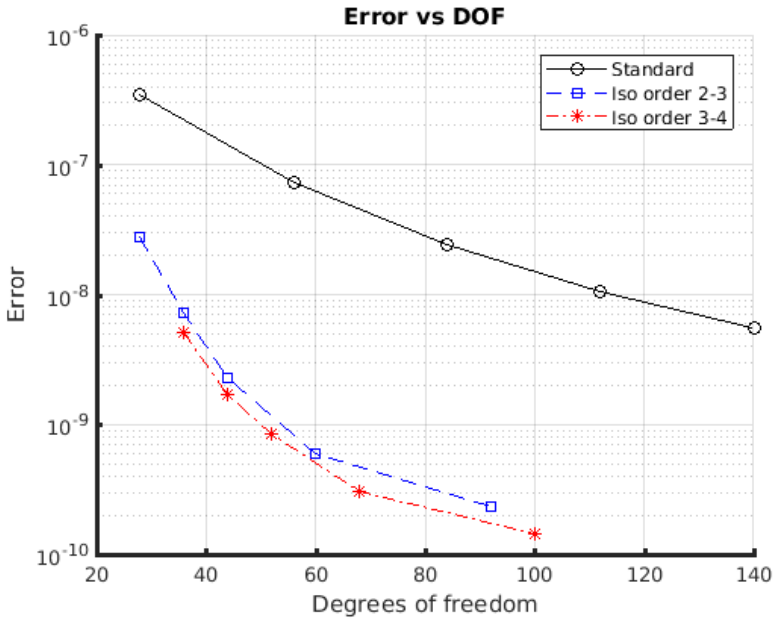

Figure 8. Displacement RMSE vs degrees of freedom for tube.

Table 4. Geometric and material properties - plate.

Property	**Symbol**	**Value**
Radius	R	50 mm
Young's Modulus	E	10^5 Pa
Poisson's ratio	ν	$0,25$
Distributed load	P	1 N/mm

by the corresponding equivalent values". This means that, for plane stress, fundamental solutions can be obtained by substituting Poisson's ratio and Young's modulus as follows:

$$\nu^{'} = \frac{\nu}{1+\nu} \tag{25}$$

$$E^{'} = E\left[1 - \frac{\nu^{'2}}{(1+\nu^{'})^2}\right] \tag{26}$$

So, after adjustment, mechanical properties of the plate become $E' = 179520$ and $\nu' = 0.2424$.

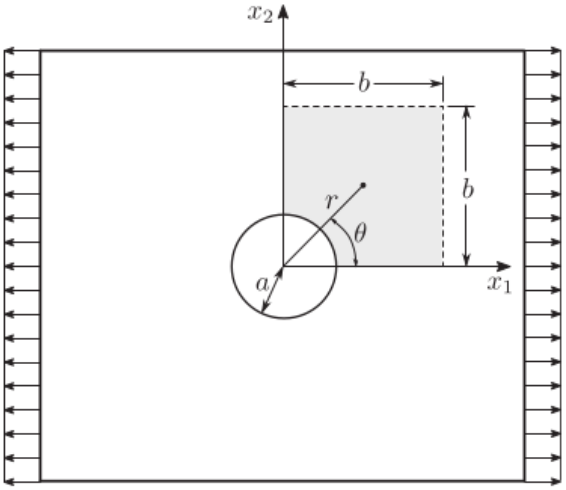

Figure 9. Boundary conditions for the plate Oliveira and Portela [25].

Figure 10 illustrates the plate with more details and boundary conditions.

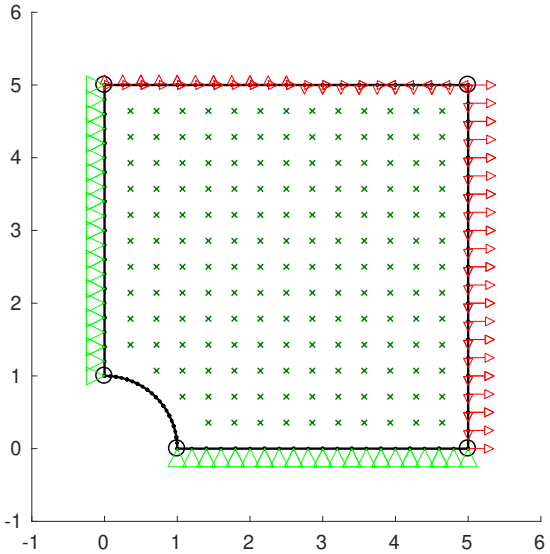

Figure 10. Detailed representation of plate with boundary conditions.

This problem has an analytical solution for stress field as follows Timoshenko et al. [23]:

$$\begin{bmatrix} \sigma_{11}(r,\theta) \\ \sigma_{22}(r,\theta) \\ \sigma_{12}(r,\theta) \end{bmatrix} = \begin{bmatrix} 1 - \frac{a^2}{r^2}(\frac{3}{2}cos(2\theta) + cos(4\theta) + \frac{3a^4}{2r^4}cos(4\theta)) \\ -\frac{a^2}{r^2}(\frac{1}{2}cos(2\theta) - cos(4\theta) - \frac{3a^4}{2r^4}cos(4\theta)) \\ -\frac{a^2}{r^2}(\frac{1}{2}sin(2\theta) + sin(4\theta) + \frac{3a^4}{2r^4}sin(4\theta)) \end{bmatrix}, \tag{27}$$

where r and θ are the usual polar coordinates, centered at the centre of the hole. Exact solution for displacement (Fan et al. [26] *apud* Timoshenko et al. [23]):

$$\begin{bmatrix} u_1(r,\theta) \\ u_2(r,\theta) \end{bmatrix} = \begin{bmatrix} \frac{10a}{8G}\left\{\frac{r}{a}(\kappa+1)cos(\theta) + \frac{2a}{r}\left[(1+\kappa)cos(\theta) + cos(3\theta)\right] - \frac{2a^3}{r^3}cos(3\theta)\right\} \\ \frac{10a}{8G}\left\{\frac{r}{a}(\kappa-3)sin(\theta) + \frac{2a}{r}\left[(1-\kappa)sin(\theta) + sin(3\theta)\right] - \frac{2a^3}{r^3}sin(3\theta)\right\} \end{bmatrix}. \tag{28}$$

Surface tractions $\mathbf{t}$ represent the force acting $\mathbf{P}$ on the surface per unit area A. Let dA be an element of area on a surface and suppose that dA is subjected to a force $d\mathbf{P}$ as in Fig. 11:

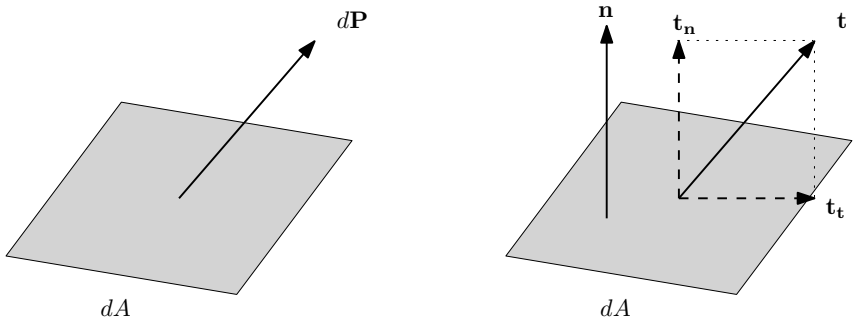

Figure 11. Surface tractions.

$$\mathbf{t} = \lim_{dA \to 0} \frac{d\mathbf{P}}{dA} \tag{29}$$

It can also be defined in terms of stress σ_{ij} and the normal vector n_j as:

$$t_i = \sigma_{ij} n_j. \tag{30}$$

Standard BEM

Simulations for the infinite plate have results in good agreement with the exact solution. It is possible to see in Fig. 12 that numerical (blue x) and analytical (red line) are close.

Table 5. Number of elements per segment for the 5 meshes - plate.

	Elem. per segment						
Mesh	1	2	3	4	5	**Total nodes**	**DOF**
SP-1	1	1	1	1	1	10	20
SP-2	2	2	2	2	2	20	40
SP-3	5	5	5	5	5	50	100
SP-4	10	10	10	10	10	100	200
SP-5	25	25	25	25	25	250	500

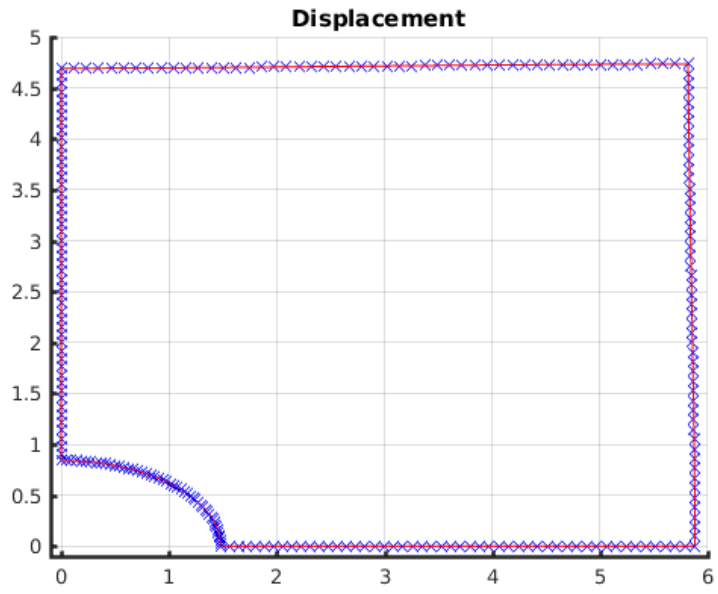

Figure 12. Displacement for plate.

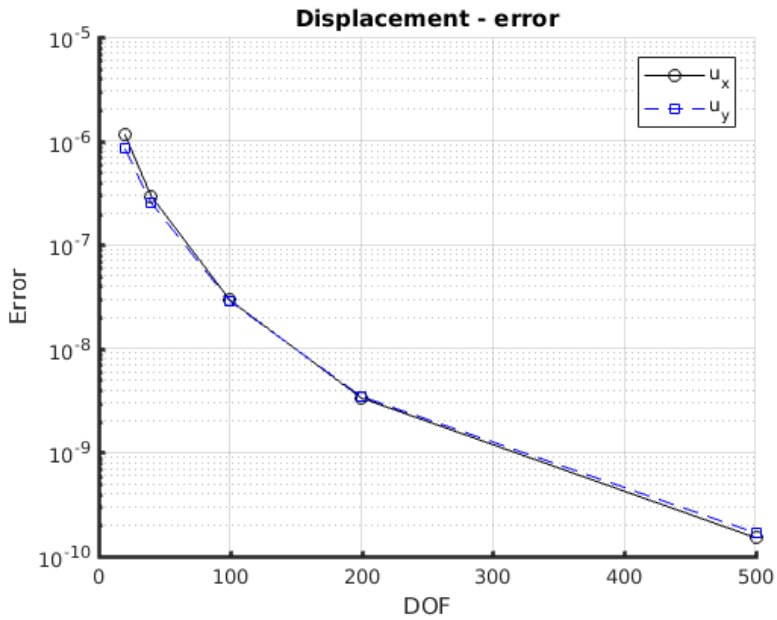

Figure 13. Displacement RMSE vs degrees of freedom for plate.

Comparing errors for displacement and tractions, it is possible to notice that tractions demand a finer mesh in relation to displacement in order to achieve the same magnitude of errors. With the coarsest mesh SP-1, displacements u_x and u_y both have error of the order of 10^{-6}. This very refined mesh produces error of about 10^{-1} for tractions. Now, looking at results from mesh SP-5, both displacements and tractions have errors smaller than 10^{-3}, which was considered acceptably low in this study.

Numerical results for stresses were also solved, and the color map is in Fig. 15. Deformed configuration was also plotted as the black line.

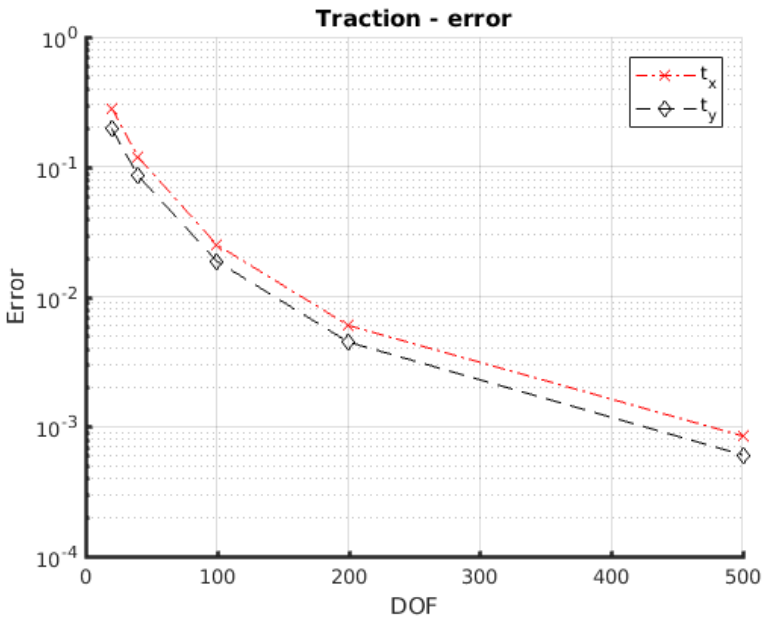

Figure 14. Tractions RMSE vs degrees of freedom for plate.

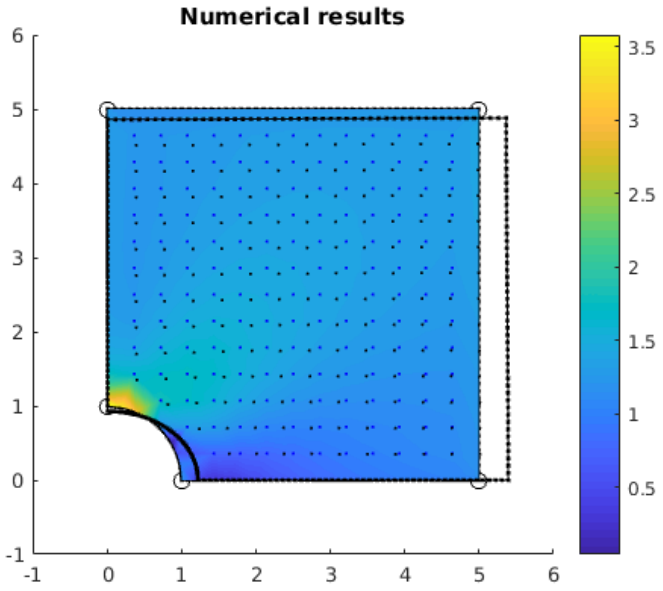

Figure 15. Stresses in plate - numerical results.

7 Conclusions

This work presented an isogeometric formulation for modelling elasticity problems and compared it to standard BEM using quadratic elements. Among the advantages of using NURBS instead of polynomials as basis for approximation of geometry and unknown fields are more accuracy and less time needed from the engineer due to a simplification or even elimination of meshing. Despite being harder to implement, IGABEM can be adapted in regular BEM codes if Bézier decomposition is made. Bézier decomposition is achieved by inserting repetead knots in knot vector, until they reach a multiplicity equals to the curve's degree. It is clear from examples that the proposed approach is more accurate when compared to quadratic elements, even with a coarser mesh.

8 Appendix A

For plane strain problems, displacement and traction fundamental solutions are given, respectively, by:

$$U_{ij}(p,Q) = \frac{1}{8\mu\pi(1-\nu)}[(3-4\nu)log\left(\frac{1}{r}\right)\delta_{ij} + r_{,i}r_{,j}] \tag{31}$$

$$T_{ij}(p,Q) = \frac{-1}{4\pi(1-\nu)r}\left\{[(1-2\nu)\delta_{ij} + 2r_{,i}r_{,j}]\frac{\partial r}{\partial n} + (1-2\nu)(r_{,i}n_j - r_j n_i)\right\}. \tag{32}$$

Acknowledgements

The first author acknowledges Program PCMEC - Pós-Graduação em Ciências Mecânicas, Department of Mechanical Engineering, Faculty of Technology, University of Brasília and for his scholarship.

References

[1] Hughes, T. J. R., Cottrell, J., & Bazilevs, Y., 2005. Isogeometric analysis: CAD, finite elements, NURBS, exact geometry and mesh refinement. *Computer Methods in Applied Mechanics and Engineering*, vol. 194, n. 39-41, pp. 4135–4195.

[2] Cottrell, J. A., Hughes, T. J. R., & Bazilevs, Y., 2009. *Isogeometric analysis: toward integration of CAD and FEA*. John Wiley & Sons.

[3] Simpson, R. N., Bordas, S. P., Trevelyan, J., & Rabczuk, T., 2012. A two-dimensional Isogeometric Boundary Element Method for elastostatic analysis. *Computer Methods in Applied Mechanics and Engineering*, vol. 209-212, pp. 87–100.

[4] Simpson, R. N., Bordas, S. P., Lian, H., & Trevelyan, J., 2013. An isogeometric boundary element method for elastostatic analysis: 2D implementation aspects. *Computers and Structures*, vol. 118, pp. 2–12.

[5] Cabral, J. J. S. P., Wrobel, L. C., & Brebbia, C. A., 1990. A BEM formulation using B-splines: I-uniform blending functions. *Engineering Analysis with Boundary Elements*, vol. 7, n. 3, pp. 136–144.

[6] Cabral, J. J. S. P., Wrobel, L. C., & Brebbia, C. A., 1991. A BEM formulation using B-splines: II-multiple knots and non-uniform blending functions. *Engineering Analysis with Boundary Elements*, vol. 8, n. 1, pp. 51–55.

[7] Temizer, I., Wriggers, P., & Hughes, T. J. R., 2011. Contact treatment in isogeometric analysis with NURBS. *Computer Methods in Applied Mechanics and Engineering*, vol. 200, n. 9-12, pp. 1100–1112.

[8] Temizer, I., Wriggers, P., & Hughes, T. J. R., 2012. Three-dimensional mortar-based frictional contact treatment in isogeometric analysis with NURBS. *Computer Methods in Applied Mechanics and Engineering*, vol. 209-212, pp. 115–128.

[9] Lu, J., 2011. Isogeometric contact analysis: Geometric basis and formulation for frictionless contact. *Computer Methods in Applied Mechanics and Engineering*, vol. 200, n. 5-8, pp. 726–741.

[10] Kiendl, J., Bletzinger, K. U., Linhard, J., & Wüchner, R., 2009. Isogeometric shell analysis with Kirchhoff-Love elements. *Computer Methods in Applied Mechanics and Engineering*, vol. 198, n. 49-52, pp. 3902–3914.

[11] Kiendl, J., Bazilevs, Y., Hsu, M. C., Wüchner, R., & Bletzinger, K. U., 2010. The bending strip method for isogeometric analysis of Kirchhoff-Love shell structures comprised of multiple patches. *Computer Methods in Applied Mechanics and Engineering*, vol. 199, n. 37-40, pp. 2403–2416.

[12] Benson, D. J., Hartmann, S., Bazilevs, Y., Hsu, M. C., & Hughes, T. J., 2013. Blended isogeometric shells. *Computer Methods in Applied Mechanics and Engineering*, vol. 255, n. November, pp. 133–146.

[13] Deng, X., Korobenko, A., Yan, J., & Bazilevs, Y., 2015. Isogeometric analysis of continuum damage in rotation-free composite shells. *Computer Methods in Applied Mechanics and Engineering*, vol. 284, pp. 349–372.

[14] Sun, Y., Trevelyan, J., Hattori, G., & Lu, C., 2019a. Engineering Analysis with Boundary Elements Discontinuous isogeometric boundary element (IGABEM) formulations in 3D automotive acoustics. *Engineering Analysis with Boundary Elements*, vol. 105, n. September 2018, pp. 303–311.

[15] Sun, S. H., Yu, T. T., Nguyen, T. T., Atroshchenko, E., & Bui, T. Q., 2018. Structural shape optimization by IGABEM and particle swarm optimization algorithm. *Engineering Analysis with Boundary Elements*, vol. 88, n. May 2017, pp. 26–40.

[16] Sun, F. L., Dong, C. Y., Wu, Y. H., & Gong, Y. P., 2019b. Fast direct isogeometric boundary element method for 3D potential problems based on HODLR matrix. *Applied Mathematics and Computation*, vol. 359, pp. 17–33.

[17] Sun, F. L., Dong, C. Y., & Yang, H. S., 2019c. Isogeometric boundary element method for crack propagation based on Bézier extraction of NURBS. *Engineering Analysis with Boundary Elements*, vol. 99, n. September 2018, pp. 76–88.

[18] Brebbia, C. A. & Dominguez, J., 1994. *Boundary elements: an introductory course*. WIT press.

[19] Katsikadelis, J. T., 2016. *The Boundary Element Method for Engineers and Scientists*. Second edi edition.

[20] Cruse, T. A., 1969. Numerical solutions in three dimensional elastostatics. *International Journal of Solids and Structures*, vol. 5, n. 12, pp. 1259–1274.

[21] Piegl, L. & Tiller, W., 1997. *The NURBS book*. Springer-Verlag Berlin Heidelberg, 2nd edition.

[22] Borden, M. J., Scott, M. A., Evans, J. A., & Hughes, T. J. R., 2011. Isogeometric finite element data structures based on Bézier extraction of NURBS. *International Journal for Numerical Methods in Engineering*, vol. 87, n. 1-5, pp. 15–47.

[23] Timoshenko, S. P., Goodier, J. N., & Abramson, H. N., 1970. Theory of elasticity. *Journal of Applied Mechanics*, vol. 37, pp. 888.

[24] Brebbia, C. A. & Dominguez, J., 1977. Boundary element methods for potential problems. *Applied Mathematical Modelling*, vol. 1, n. 7, pp. 372–378.

[25] Oliveira, T. S. & Portela, A., 2016. Weak-form collocation – A local meshless method in linear elasticity. *Engineering Analysis with Boundary Elements*, vol. 73, n. April, pp. 144–160.

[26] Fan, L., Coombs, W. M., & Augarde, C. E., 2018. The point collocation method with a local maximum entropy approach. *Computers and Structures*, vol. 201, n. May 2019, pp. 1–14.